Empirical potential for methyl-radical association with diamond surfaces

Pascal de Sainte Claire and William L. Hase
Department of Chemistry, Wayne State University, Detroit, Michigan 48202
(Received 16 September 1996)

An analytical potential-energy function for $\cdot CH_3$ association with carbon-atom radical sites on diamond surfaces is derived from experimental energies, structures, and vibrational frequencies, high-level *ab initio* calculations, and properties of potential-energy functions for $H\cdot + \cdot CH_3$, $\cdot CH_3 + \cdot CH_3$, and $H\cdot + \cdot C(CH_3)_3$ association. This $\cdot CH_3$+diamond potential-energy function is a molecular anharmonic potential written with switching (MAPS) functions and is identified by MAPS/MeDIAM. It is a sum of lattice (V_{lattice}), nonbonded ($V_{\text{nonbonded}}$), and radial site ($V_{CH_3,\text{site}}$) potential terms. There are many general properties of potential-energy functions for alkyl radical association reactions which are transferable and can be used to help construct $V_{CH_3,\text{site}}$. Additional properties of $V_{CH_3,\text{site}}$ are determined by *ab initio* calculations using the restricted and unrestricted quadratic configuration-interaction method, with single, double, and perturbative triple excitations and the 6-31G** basis set. The MAPS/MeDIAM potential function is used to study $\cdot CH_3$ association with a carbon-atom radical site on the diamond {111} terrace. The energy for $\cdot CH_3$ adsorption with this site is calculated to be 17 kcal/mol lower than the *ab initio* CH_3-$C(CH_3)_3$ bond dissociation energy. A canonical variational transition-state theory calculation, based on the MAPS/MeDIAM potential, gives a value of 0.06 10^{13} $cm^3\,mol^{-1}\,s^{-1}$ for the $\cdot CH_3$+diamond {111} terrace site association rate constant at 1500 K. A linear free-energy relationship is shown for the kinetics of $\cdot H$ and $\cdot CH_3$ association with a diamond {111} terrace site. [S0163-1829(97)07132-4]

I. INTRODUCTION

The extreme structural, electrical, and optical properties of diamond are responsible for its uniqueness and its high technological importance; e.g., its use in optical windows, capacitors, abrasives, and heat exchangers. Recent years have seen the emergence of chemical vapor deposition (CVD) (Refs. 1–9), methods for producing diamond films of specific type and thickness. In low-pressure CVD methods, a mixture of a small percentage of a hydrocarbon such as CH_4 and molecular hydrogen is often vaporized over a hot filament and then condensed on a colder substrate. Global chemical mechanisms, based on kinetic observations, have been proposed[10–12] for the diamond growth, and detailed analyses of elementary reactions[9,13–19] involved in the deposition process have recently been reported. Important reactions in the mechanisms are

$$H\cdot + H\text{-}C_d \rightarrow H_2 + \cdot C_d \tag{1}$$

$$H_3C\cdot + H\text{-}C_d \rightarrow CH_4 + \cdot C_d \tag{2}$$

$$H\cdot + \cdot C_d \rightarrow H\text{-}C_d \tag{3}$$

$$H_3C\cdot + \cdot C_d \rightarrow CH_3\text{-}C_d \tag{4}$$

where $\cdot C_d$ represents a carbon radical site on a diamond surface. Steps (1) and (2) produce radical sites, step (3) is responsible for site decay, and step (4) is widely accepted as a key elementary step in diamond growth.

Both experimental[20,21] and theoretical[22–25] kinetic data for reactions (1) and (3) have recently been reported. Adsorption of a radical species such as $\cdot CH_3$ to diamond radical sites has been modeled by postulating a chemical similarity[26] between gas-phase and gas-surface reactions,[27,28] where the diamond surface is considered to be a large alkane. It is argued that elementary reactions on diamond surfaces are localized at carbon sites,[26] as is the case for gas-phase hydrocarbon reactions. Though the kinetics of CVD diamond growth have been modeled with gas-phase hydrocarbon elementary reactions,[29,30] the overall validity of this approach has not yet been established. However, a recent theoretical/computational study[22,23] suggests that the postulate of chemical similarity is valid for reaction (3). Probing the postulate of chemical similarity involves understanding reaction mechanisms at the microscopic level.

The lack of experimental data is a critical problem in modeling CVD diamond growth, especially when considering methyl adsorption, reaction (4). This is thought to be a key step in the growth process, adding a quaternary center to the surface. Methyl-radical-based mechanisms are numerous. The Tsuda-Nakajima-Oikawa[31] mechanism involves adsorption of three neighboring $\cdot CH_3$ species on a {111} diamond surface, whereas $\cdot CH_3$ addition to reconstructed {100} dihydride,[32] reconstructed {100} monohydride,[19] or {110} surface sites[33] are important steps in other mechanisms invoked for diamond growth. Similarly, a combined methyl-acetylene mechanism[25,27] involves methyl radical addition to a {111} diamond surface radical site.

In the work reported here, the postulate of chemical similarity is found to be valid for alkyl radical association reactions, and is used to develop an analytic function to represent the potential-energy surface (PES) for reaction (4). The form of the analytic function is similar to that used previously to represent the PES for H-atom association with radical sites on diamond surfaces,[22] and is written as

$$V = V_{\text{lattice}} + V_{CH_3,\text{site}} + V_{\text{nonbonded}}. \tag{5}$$

This is a molecular anharmonic potential written with switching MAPS (Ref. 34) functions and is called a MAPS/MeDIAM potential.

V_{lattice} in Eq. (5) is a valence force field potential that has been fit to the diamond phonon spectrum.[35] It was used in modeling the PES for H-atom association with radical sites on diamond surfaces.[22,23] $V_{\text{nonbonded}}$ represents the nonbonded interactions between the methyl radical being adsorbed and the lattice atoms. $V_{\text{CH}_3,\text{site}}$ represents the interaction between a methyl radical and a localized carbon-atom radical site on the diamond surface. As for the H-atom diamond surface potential,[22] the carbon-atom radical site is modeled by a constrained *t*-butyl radical whose three carbon atoms, attached to the radical carbon, are kept at a fixed geometry corresponding to equilibrium positions of bulk diamond. Parameters for $V_{\text{CH}_3,\text{site}}$ are deduced from similarities between potential surface parameters for alkyl radical association and *ab initio* calculations for the association of $\cdot CH_3$ with the constrained *t*-butyl radical. The *ab initio* calculations are performed with a Gaussian series of programs,[36] using both the restricted and unrestricted quadratic configuration interaction method with single, double, and perturbative triple excitations; i.e., QCISD(T).[37] The 6-31G** extended basis set of the split-valence type was used.

A radical-radical recombination process, such as $\cdot CH_3$ association with a radical site on a diamond surface, is barrierless,[38] and a variational version of transition-state theory[39] must be used to calculate the association rate constant. In canonical variational transition-state theory (CVTST), the transition state (TS) is located at the free-energy maximum along the reaction path. For $H\cdot + \cdot CH_3$ and H· +diamond{111} association,[22,40] CVTST calculations based on the reaction path Hamiltonian[41–43] give rate constants in excellent agreement with those determined from classical trajectory calculations. Long-range interactions were found to be responsible for the large intermolecular distances at the variational transition states. In the work presented here, the PES derived for reaction (4) is used with the CVTST/reaction path Hamiltonian calculational approach to determine a rate constant for $\cdot CH_3$ association with a carbon-atom radical site on the diamond{111} surface.

II. PREVIOUS WORK

Understanding the elementary process of methyl radical association with a diamond surface radical site requires knowledge of the reaction's multidimensional PES. In deriving such a PES, information is needed about radical and angular deformations, as well as equilibrium bond lengths and angles, and force constants for the numerous degrees of freedom involved. Several methods have been used to derive PES's for reactions involving diamond surfaces.[22,23,44–63] The large number of atoms involved is a serious limitation when simulating bulk diamond and, thus, approximations in the method and/or limitations in the number of atoms treated are common.

Ab initio[22,44–50] and local-density-approximation-based[51] calculations have been performed on small hydrocarbon clusters to model reactions on diamond surfaces. Abstraction and bond dissociation energies,[44,45,47–51] relaxation of the surface radical site,[50,51] and transition state geometries have been determined from these calculations. For H-atom association with a surface radical site, a complete PES (Ref. 22) was derived. These calculations generally require extensive computer time, and the number of basis functions becomes a critical issue as the size of the hydrocarbon cluster model increases.

Semiempirical quantum chemical calculations[32,52,53] which include electron correlation have also been used to model diamond surface reactions. Though a good overall description of the PES is often obtained, this method is not as accurate as the *ab initio* and density-functional-type methods. However, it is less computationally expensive, and can be used to study large model systems. Semiempirical calculations have been particularly useful for comparing relative energies of reaction intermediates involved in diamond growth mechanisms.[33,52] Reaction path following calculations using semiempirical PES's has not been reported for diamond surface reactions.

Empirical potentials[54,55] with parameters fit to known experimental data, such as bond energies, abstraction energies, heats of formation, and lattice constants, have been derived over the past decade. The many-body Brenner[56] potential for hydrocarbons has been extensively used in modeling diamond surfaces. Though inclusion of conjugation effects and its applicability to any diamond surface reaction involving carbon and hydrogen atoms makes it very appealing, long-range interactions involved in bond-breaking or-forming processes are not well described.[57] This is essentially a consequence of the need for cutoff parameters, which restrict the interactions between atoms within a short atomic radius. Similar to this approach, class-I and -II force fields[58] for hydrocarbons have been used in the simulations of many hydrocarbons [e.g., the AMBER,[59] CHARMM,[60] CVFF,[61] MM3,[54] and CFF93 (Ref. 62) force fields], but again long-range covalent interactions are not described accurately. This is a consequence of restricting the data included in fitting the force fields to only equilibrium structure properties. A recent approach that involves fitting an alkane PES to a somewhat wider range of *ab initio* data has been developed and is known as a quantum mechanical-force field (QMFF).[63] But one faces the same problem, especially for radical-radical recombination reactions, for which very long-range interactions are of critical importance.

The results of high-level *ab initio* calculations have been used to develop accurate potential energy surfaces for the three alkyl radical association reactions[22,45,47]

$$H\cdot + \cdot CH_3 \rightarrow CH_4, \tag{6}$$

$$\cdot CH_3 + \cdot CH_3 \rightarrow CH_3\text{-}CH_3, \tag{7}$$

$$H\cdot + \cdot {}^t\text{Bu} \rightarrow \text{H-}{}^t\text{Bu}. \tag{8}$$

The calculations were based on the configuration-interaction (CI) method,[64] which treats instantaneous correlations between motion of the electrons, and used the 6-31G** basis set. A limited number of calculations for reaction (8) were also performed with the much larger 6-311 $++G(3df,3pd)$ basis set.[22] The CI calculations included single and double excitations for reaction (6),[45] single, double, and quadruple excitations for reaction (7),[47] and

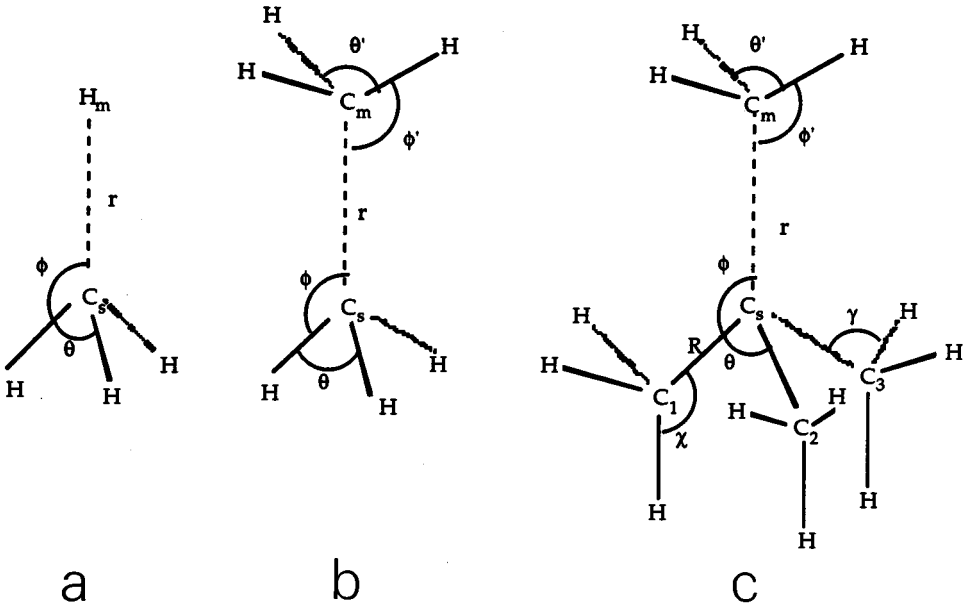

FIG. 1. Internal coordinates of the model clusters used to describe reactions (6), (7), and (8).

single, double, triple, and quadruple excitations for reaction (8).[22] The positions of the nonradical carbon atoms in the *t*-butyl radical of reaction (8) were held fixed to model the geometry of bulk diamond, and the results of the *ab initio* calculations were used to derive an analytic PES for H-atom association with carbon-atom radical sites on diamond surfaces.[22]

A comparison of the *ab initio* potential-energy surfaces for reactions (6)–(8) allows one to investigate the postulate of chemical similarity. For reactions (6) and (7), the adsorbing species change from $\cdot$H to $\cdot CH_3$ and the substrate changes from $\cdot CH_3$ to $\cdot {}^t$Bu for reactions (6) and (8). If there are fundamental similarities between the potential-energy surfaces for these reactions, with transferrable parameters, it may be possible to use this information to derive a PES for

$$CH_3\cdot + \cdot {}^t\mathrm{Bu} \rightarrow CH_3\text{-}{}^t\mathrm{Bu}. \tag{9}$$

If the geometry of the *t*-butyl radical in Eq. (9) is constrained, as described above, to represent bulk diamond, the resulting PES is that for $V_{CH_3,site}$ in Eq. (5). In the following, it is shown that it is possible to use properties of the potential energy surfaces for reactions (6) and (7) to modify the PES for reaction (8) and determine detailed properties of the PES for reaction (9).

III. PARAMETERS FOR $V_{CH_3,site}$ FROM PES PROPERTIES FOR REACTIONS (6)–(8)

A. Model for $V_{CH_3,site}$

The models and coordinates used to describe the potential-energy functions for reaction (6) and (7) and $V_{CH_3,site}$ for reactions (4) and (9) are shown in Fig. 1. The radical site is denoted $\cdot C_s$ and dashes represent the forming bond. The methyl radical carbon atom is represented by $\cdot C_m$. The nomenclature for the models is consistent with previous studies.[22,45,47] The model species used to model $V_{CH_3,site}$ is a constrained *t*-butyl radical (t-C_4H_9) where the carbon atoms C_1, C_2, and C_3 are held fixed [Fig. 1(c)]. This species has been successfully used in a previous study of H-atom addition to diamond surfaces.[22]

When alkyl radicals associate there are relaxations about the carbon-atom radicals as a result of the transition from sp^2 and sp^3 electron configuration. A similar type of relaxation occurs for the constrained *t*-butyl radical (or a radical site on a diamond surface), with the radical carbon-atom $\cdot C_s$ moving toward the entity being adsorbed. For the potential-energy functions used to represent reactions (6)–(8), this relaxation is written as a function of r (see Fig. 1) and the same is done here for $V_{CH_3,site}$. Thus, the three C_m—C_s-C angles ϕ_i (bending motion of the methyl radical with respect to the *t*-butyl radical C_{3v} symmetry axis), the three C-$C_s\cdot$-C angles θ_i, the three H-C_m—C_s angles ϕ_i' (rocking motion of the methyl radical about the C_m—C_s axis), and the three H-C_m-H angles θ_i' have ''equilibrium'' values, noted $\phi_o(r)$, $\theta_o(r)$, $\phi_o'(r)$, and $\theta_o'(r)$, respectively, which depend on r. Similarly, the γ_i (six $\cdot C_s$-C-H angles), χ_i (three $\cdot C_s$-C-H angles), and R_i (three $\cdot C_s$-C bond distances) have respective ''equilibrium'' values $\gamma_o(r)$, $\chi_o(r)$, and $R_o(r)$. The out-of-plane motion of the methyl radical is defined by the angle Δ and is also a function of r. Its definition is taken to be identical to that in Ref. 44, Eq. (15). As shown below, expressions for the $V_{CH_3,site}$ ''equilibrium'' coordinates versus r may be deduced from analogous expressions for reactions (6)–(8).

Several $V_{CH_3,site}$ bending force constants are attenuated as the C_m—C_s distance between the surface radical site and the methyl carbon atom increases; i.e., $f_\phi(r)$, $f_{\phi'}(r)$, $f_{\theta'}(r)$, and $f_\Delta(r)$, the C_m—C_s-C, H-C_m—C_s, H-C_m-H bending, and C_mH_3 out-of-plane bending force constants, respectively. These force constants are attenuated between their values when the methyl radical is attached to the site, in its equilibrium geometry, and their values at a large C_m—C_s separation. The $f_\phi(r)$ and $f_{\phi'}(r)$ force constants become zero at large C_m—C_s separations, and $f_\Delta(r)$ is zero when the

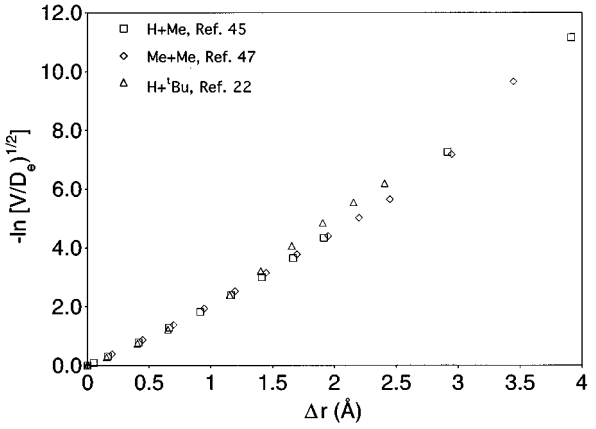

FIG. 2. Plots of $-\ln[1-(V/D_e)^{1/2}]$ vs Δr, the elongation of the H-C or C-C bond, for the different association reactions studied here.

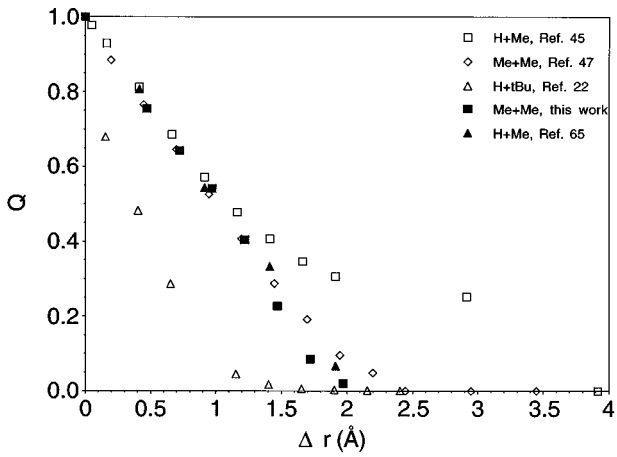

FIG. 3. Plots of the reduced angle function $Q(\Delta r)$ as a function of Δr for the different association reactions. Δr is defined in Fig. 2.

methyl radical is attached to the surface site. The remaining limiting values for the force constants are nonzero.

B. Radial potential

The radial part of the potential-energy surfaces for reactions (6)–(8) are examined first, i.e., the dependence of the PES on the C_m—C_s (or H_m—C_s) distance r (see Fig. 1). A widely used analytical form of such a radial interaction is the Morse function

$$V(r)=D_e[1-\exp(-\beta\Delta r)^2, \tag{10}$$

where D_e is the classical bond dissociation energy and $\Delta r = r-r_0$. Plots of $-\ln[1-(V/D_e)^{1/2}]$ versus Δr are given in Fig. 2 for reactions (6), (7), and (8). The $V(r)$ are the *ab initio* radial potentials from Refs. 22, 45, and 47. D_e and r_o are 109.46 kcal/mol and 1.090 Å for reaction (6),[45] 93.97 kcal/mol, and 1.552 Å for reaction (7),[47] and 104.94 kcal/mol and 1.095 Å for reaction (8).[22] The curves for reaction (6) and (7) are identical, which means the form of β is the same for each. The curve for reaction (8) is slightly different, which may be caused by constraining the *t*-butyl radical.

The independence of the $V(r)/D_e$ potential with respect to the size of the hydrocarbon radical (here H· and $\cdot CH_3$) associating with $\cdot CH_3$ is an important result and suggests the same may be true for association with the constrained *t*-butyl radical. Thus, the reduced potentials $V(r)/D_e$ for reactions (8) and (9) are assumed to be the same, with β given by the quartic polynomial determined previously for reaction (8),[22] i.e.,

$$\beta=\beta_e+c_2\Delta r+c_3\Delta r^2+c_4\Delta r^3+c_5\Delta r^4, \tag{11}$$

where $\beta_e=1.852$ Å^{-1}, $c_2=-1.350\,593\,72$ Å^{-2}, $c_3=2.282\,349\,51$ Å^{-3}, $c_4=-1.000\,421\,23$ Å^{-4}, and $c_5=0.137\,143\,873$ Å^{-5}. D_e and r_o for reaction (9), with a constrained *t*-butyl radical to represent $V_{CH_3,site}$ are given below in Sec. IV.

C. Relaxation of important angles

As discussed above, when the methyl radical associates with a radical site on the diamond surface, several angle relaxations occur, namely, $\phi(r)$, $\theta(r)$, $\gamma(r)$, $\chi(r)$, $\phi'(r)$, and $\theta'(r)$, as well as the bond relaxations $R(r)$ [see Fig. 1(c)]. Equilibrium values for these coordinates versus r can be expressed by

$$X_o(r)=X_\infty+(X_{\rm eq}-X_\infty)S_{\Delta X}(r), \tag{12}$$

where $X_o(r)$ is the equilibrium value of the coordinate X versus r, X_∞ is the equilibrium value of X as r approaches infinity, $X_{\rm eq}$ is the equilibrium value of X when the methyl radical has associated and is in its potential-energy minimum, and $S_{\Delta X}(r)$ is a switching function that connects X_∞ and $X_{\rm eq}$ and represents the attenuations of the relaxations. Since $\theta_o(r)$, $\gamma_o(r)$, $\chi_o(r)$, $\theta'_o(r)$, and $R_o(r)$ may be directly related to $\phi_o(r)$ and $\phi'_o(r)$, only these two latter angles need be examined. From geometrical considerations the following relationships can be derived;

$$\theta_o(r)=A\,\cos\{1-\tfrac{3}{2}\,\sin^2[\pi-\phi_o(r)]\}, \tag{13}$$

$$\gamma_o(r)=A\,\cos\{\tfrac{1}{2}\,\sin[\phi_o(r)-\tau]\sin\,\tau + \cos[\phi_o(r)-\tau]\cos\,\tau\}, \tag{14}$$

$$\chi_o(r)=\phi_0(r), \tag{15}$$

$$R_o(r)=R_o(r_o)\frac{\sin[\phi_o(r_o)]}{\sin[\phi_o(r)]}, \tag{16}$$

$$\theta'_o(r)=A\,\cos\{1-\tfrac{3}{2}\,\sin^2[\pi-\phi'_o(r)]\}, \tag{17}$$

where τ is the tetragonal angle 109°28′. To speed up trajectory calculations using these functions, they may be fit to simpler functional forms.[44]

1. ϕ relaxation

The function $\phi_o(r)$ describes the relaxation of the radial site. The function $Q(\Delta r)=[\phi_o(r)-\phi_\infty]/[\phi_{\rm eq}-\phi_\infty]$ allows site relaxations to be compared for different association reactions. $Q(\Delta r)$ is plotted versus $\Delta r=r-r_o$ in Fig. 3 for reactions (6), (7), and (8). The points in Fig. 3 for $H\cdot+\cdot CH_3$, i.e., reaction (6), are from the MRD CI/6-31G** calculations of Hirst[45] and the multirelevence determinant (MRD) CI/6-

311++G(df,p) calculations of Brown and Truhlar.[65] Both use 11 reference configurations. These two sets of calculations begin to diverge at $\Delta r=1$ Å and differences become important for Δr larger than 1.5 Å. A careful look at Tables 1 and 2 of the work by Hirst[45] shows some inconsistencies. In Table 1, Hirst reported values for $\phi_o(r)$ and energies for the optimized geometries. In Table 2 energies calculated for the optimized structures of Brown and Truhlar[65] were reported. The energies in Table 2 are lower than those in Table 1, suggesting that the structures obtained by Brown and Truhlar are the true optimized geometries.

The points in Fig. 3 for methyl radical association, i.e., reaction (7), are from the MRD CI/6-31G** (two reference configurations) calculations of Robertson *et al.*[47] and additional calculations performed here at the UQCISD(T)/6-31G** level of theory.[66,67] These two sets of calculations are in good agreement and agree with the H·+ ·CH_3 $Q(\Delta r)$ curve obtained from Brown and Truhlar's results. Thus, the function $Q(\Delta r)$ is the same for H· and ·CH_3 association with ·CH_3. As a result of this finding, $Q(\Delta r)$ was also assumed to be the same for H· and ·CH_3 association with the constrained ^{t}Bu radical. Thus $S_{\Delta\phi}(r)$ in Eq. (12) is assumed equivalent to $Q(\Delta r)$ for reaction (8), which was fit previously[22] to give

$$\frac{\phi_o(r)-\phi_\infty}{\phi_{\rm eq}-\phi_\infty}=S_{\Delta\phi}(r), \tag{18}$$

$$S_{\Delta\phi}(r)=A\ \exp(-B\Delta r^2)+(1-A)\exp(-C\Delta r^2), \tag{19}$$

where $A=0.355\,275\,203$, $B=83.216\,231\,9$ Å^{-2}, $C=2.022\,269\,04$ Å^{-2}. Values of $\phi_{\rm eq}$ and ϕ_∞ for reaction (9), i.e., $V_{\rm CH_3,site}$ are presented in Sec. IV.

2. ϕ' and θ' relaxation

The above analysis shows that relaxation of the ·CH_3 geometry is the same for ·CH_3 addition to H· and ·CH_3. Thus the same geometry relaxation is assumed for ·CH_3 addition to the ^{t}Bu radical. As shown in Fig. 1, the two ·CH_3 angle coordinates which relax are $\phi'_o(r)$ and $\theta'_o(r)$. Their relaxations are taken to be the same as those for the association of two methyl radicals,[47] which are given by

$$\frac{\phi'_o(r)-\phi'_\infty}{\phi'_{\rm eq}-\phi'_\infty}=S_{\Delta\phi'}(r), \tag{20}$$

$$S_{\Delta\phi'}(r)=1-\tanh\{\lambda_{\Delta\phi'}\Delta r[\exp(\gamma_{\Delta\phi'}\Delta r^3)+1]\}, \tag{21}$$

$$\frac{\theta'_o(r)-\theta'_\infty}{\theta'_{\rm eq}-\theta'_\infty}=S_{\Delta\theta'}(r), \tag{22}$$

$$S_{\Delta\theta'}(r)=1-\tanh\{\lambda_{\Delta\theta'}\Delta r[\exp(\gamma_{\Delta\theta'}\Delta r^3)+1]\}, \tag{23}$$

where $\lambda_{\Delta\phi'}=0.27$ Å^{-1}, $\gamma_{\Delta\phi'}=0.078$ Å^{-3}, $\lambda_{\Delta\theta'}=0.45$ Å^{-1}, and $\gamma_{\Delta\theta'}=0.089$ Å^{-3}. $\phi'_{\rm eq}$, ϕ'_∞, $\theta'_{\rm eq}$, and θ'_∞ are presented in Sec. IV.

D. Attenuation of ϕ and ϕ' force constants

Two ϕ-type bending forces are attenuated as the C—C bond between ·CH_3 and ·^{t}Bu in reaction (9) is stretched; i.e., the H-C_m—C_s-Cϕ' and C_m—C_s-Cϕ bending forces (see Fig. 1). There is considerable interest in such bending force constant attenuations.[46,68] From *ab initio* calculations, similar force-constant attenuations were found for the H—C-H bend in methane and the H—C-C bends in ethylene and propylene, upon elongation of the H—C bond.[46] However, for the isobutane H—C-C bend, with the constrained *t*-butyl radical, the *ab initio* force constant attenuation is different. These *ab initio* force constant attenuations for methane and isobutane, which pertain to reaction (6) and (8), respectively, are given in Fig. 4 in the form $S_\phi(\Delta r)=f_\phi(r)/f^o_\phi$, where f^o_ϕ is the force constant at the equilibrium geometry and $\Delta r=r-r_o$ is the displacement of the stretched bond from its equilibrium value. These $S_\phi(\Delta r)$ for reactions (6) and (8) are plots of Eqs. (1) and (21) in Refs. 46 and 22, respectively. The attenuation of the H—C-H f_ϕ for reaction (6) is seen to be somewhat more pronounced than that of the H—C-C f_ϕ for reaction (8). In contrast, the methane H—C-H attenuation is very similar to the H—C-C f_ϕ attenuations for ethylene and propylene.[46] For each of these force-constant attenuations, the complete geometry of the system was optimized, without any constraints, as the H—C bond was stretched. However, for H·+·^{t}Bu, reaction (8), part of the ^{t}Bu geometry is constrained and held at positions different that those for the completely optimized geometry. This constraint may contribute anharmonic forces to the ϕ-bending potential, which affect the attenuation of the f_ϕ force constant.

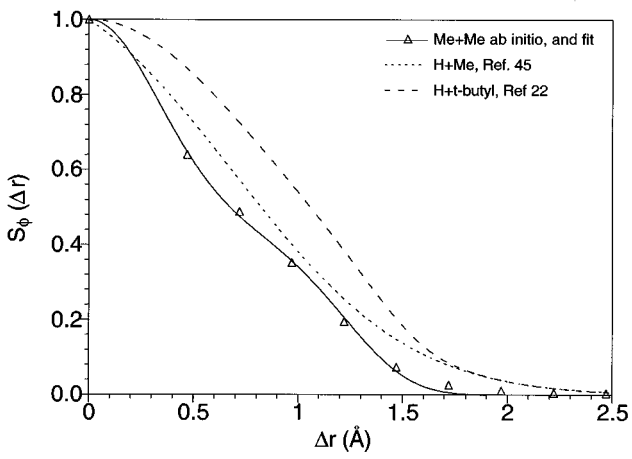

FIG. 4. Plots of $S_\phi(\Delta r)$ for different association reactions. Δr is defined in Fig. 2.

The above analysis suggests that the H-C_m—C_s ϕ' and C_m—C_s-C ϕ bends for ·CH_3+·^{t}Bu, reaction (9), should have different force-constant attenuations. The ϕ' bend does not contain a constrained atom, while the position of the lattice C atom is constrained for the ϕ bend. Because of the similar H—C-H and H—C-C force-constant attenuations for methane, ethylene, and propylene, the attenuations of the H-C_m—C_s ϕ' force constant for reaction (9) and the H-C—C ϕ force constant for ethane were assumed to be the same. This latter force-constant attenuation was determined by UQCISD(T)/6-31G** *ab initio* calculations. The C_2H_6 geometry was first optimized at fixed C—C distances r to give $\phi_o(r)$. Then only the H-C—C ϕ angles for one of the methyl groups were displaced by changing one of these angles by 5° [see Fig. 1(b)]. The resulting bending energy $E_\phi(r)$, which is

TABLE I. Methyl radical recombination UQCISD(T)/6-31G** ϕ-bending energies and force constants $f_\phi(r)$.

r[a]	E_{radical}[b]	ϕ_o	f_ϕ[c]
1.5286	−96.0838	111.15	0.8455
2.0	−63.1921	105.97	0.5413
2.25	−41.3122	103.59	0.4130
2.5	−22.6346	101.45	0.2977
2.75	−9.6863	98.55	0.1646
3.0	−3.8145	94.80	0.6263×10^{-1}
3.25	−1.7793	91.81	0.2204×10^{-1}
3.5	−0.9900	90.44	0.9086×10^{-2}
3.75	−0.5922	89.94	0.4179×10^{-2}
4.0	−0.3469	89.64	0.3056×10^{-2}
7.0	6.4×10^{-3}	90.00	

[a]C_m—C_s intermolecular distance [see Fig. 1(b)] in Å.
[b]Radial energy in kcal/mol.
[c]Force constant associated with the ϕ motion in mdyn Å/rad^2; see Eq. (24).

the difference between the energy for the optimized geometry and that with the ϕ angles displaced, was then fit to

$$E_\phi(r)=\frac{f_\phi(r)}{2}\sum_{i=1}^{3}[\phi_i-\phi_o(r)]^2 \tag{24}$$

to give $f_\phi(r)$. The optimized geometries, potential energies, and f_ϕ, versus r, are listed in Table I. Since fitting $f_\phi(r)$ involves computing the difference between two UQCISD(T) energies, the small spin contamination[69] is assumed to cancel. Because of the larger number of electrons and, thus, more significant spin contamination, calculations of this type were not performed to determine bend attenuations for the ^{t}Bu—CH_3 system. For large C—C separations, the spin contamination was large and the calculated attenuated force constants could not be considered as reliable.

The attenuation of the ethane H-C—Cϕ force constant, i.e., $S_\phi(\Delta r)=f_\phi(r)/f_\phi^o$, was fit to represent the attenuation of the H-C_m—$C_s\phi'$ force constant for reaction (9). The resulting fit for $S_{\phi'(r)}$ is

$$S_{\phi'}(r)=a_1\exp(-b_1\Delta r^2)+(1-a_1)\exp(-b_2\Delta r^5)\quad\text{for } r\geqslant r_o \tag{25}$$

$$S_{\phi'}(r)=1\quad\text{for } r\leqslant r_o,$$

with $a_1=0.554\,627\,039\,53$, $b_1=4.479\,320\,631\,4$ Å^{-2}, and $b_2=0.284\,328\,737\,2$ Å^{-5}.[70] Figure 4 shows that Eq. (25) provides an excellent fit to the *ab initio* $f_\phi(r)/f_\phi^o$ values for ethane.

As shown in Fig. 4, the attenuations of the ethane H-C—C and methane H-C—H ϕ force constants are similar, and also like those for the ethylene and propylene C-C—H ϕ force constants.[46] Each of these four attenuations were determined by optimizing the system's geometry as the C—H or C—C bond was stretched. The similarity between these f_ϕ attenuations supports the concept of transferable potential-energy functions and parameters for related chemical systems.

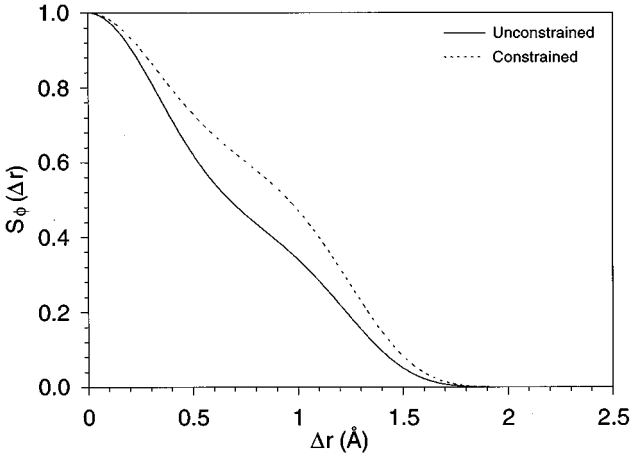

FIG. 5. Plots of $S_\phi(\Delta r)$ for the H-C—C bend in ethane (—), and the scaled $S_\phi(\Delta r)$ that mimics CH_3 association with a constrained ^{t}Bu radical (– – –) (see text). Δr is defined in Fig. 2.

Two different approaches were used to model the attenuation for the CH_3-^{t}Bu C_m—C_s-C ϕ force constant. For the first, the attenuation of this force constant was assumed to be the same as for the H-C_m—C_s ϕ' force constant; i.e., Eq. (25). This model does not include any possible effects that constraining the lattice C atoms may have on the attenuation of the C_m—C_s-C ϕ force constant.

For the second approach, it was assumed that the ratio of the attenuations for the C_m—C_s-C ϕ and H-C_m—C_s ϕ' force constants for CH_3—^{t}Bu is the same as the ratio of the attenuations of the H-^{t}Bu H—C-C and methane H—C-H ϕ force constants. Both the C_m—C_s-C and H-^{t}Bu H—C-C ϕ force constants involve a constrained ^{t}Bu radical. The resulting attenuation for the C_m—C_s-C f_ϕ is also given by Eq. (25), but with the parameters $a_1=0.390\,620\,534\,28$, $b_1=4.528\,131\,028\,3$ Å^{-2}, and $b_2=0.262\,492\,796\,38$ Å^{-5}. A possible shortcoming of this model is that effects of the geometry constraints may be less important for CH_3-^{t}Bu than for H-^{t}Bu. This is because the CH_3-^{t}Bu tetrahedral minimum energy geometry is the same as that for the diamond lattice, while H-^{t}Bu must be constrained at this geometry for its potential minimum.

The attenuations for these two models of the C_m—C_s-C ϕ force constant are compared in Fig. 5. It is expected that the actual attenuation is intermediate between these two curves. The effect of these different attenuations, on the CH_3+diamond{111} association rate, is discussed below. Values for f_ϕ^o and $f_{\phi'}^o$ are given in Sec. IV.

IV. *AB INITIO* CALCULATIONS FOR THE CH_3-^{t}Bu ASYMPTOTIC LIMIT

The analyses presented above show that properties of the potential-energy surfaces for reactions (6)–(8) may be used to describe the attenuations of forces and structures of the potential energy surface for reaction (9) between its two asymptotic limits, i.e., $\cdot CH_3$ and $\cdot\,^t$Bu at infinite separation and CH_3-^{t}Bu in its minimum-energy geometry. In this section, *ab initio* calculations are used to derive geometries, energies, and force constants for the CH_3-^{t}Bu asymptotic

limit. The properties of $\cdot CH_3$ and $\cdot {}^t$Bu at infinite separation have been determined in previous *ab initio* calculations.[22,44,45]

A. Geometry and energy of CH_3-^{t}Bu

The geometry and energy of the CH_3-^{t}Bu neopentanelike model [see Fig. 1(c)], with the C_1, C_2, and C_3 carbon atoms held fixed with bond lengths and angles corresponding to a diamond lattice, were calculated at the QCISD(T)/6-31G** level of theory. The C_m-H distances of the methyl moiety were fixed at the experimental neopentane C-H bond length of 1.1 Å.[71] The measure of the degree of pyramidalization about the $\cdot {}^t$Bu radical carbon is the distance R_p between C_s [Fig. 1(c)] and a plane formed by carbon atoms C_1, C_2, and C_3. The change in R_p is referred to as the relaxation of the radical site.[22,50,51] Three parameters are needed to describe the equilibrium C_{3v} geometry of the CH_3-^{t}Bu potential minimum; i.e., the C_s-C_m distance r, the site relaxation parameter R_p, and the three H-C_m-C_s angles given by ϕ'.

The CH_3-^{t}Bu equilibrium geometry, at the HF/6-31G** level of theory, was determined by analytic gradients. Energies for this geometry and displacements away from it were then calculated at the QCISD(T)/6-31G** level of theory. These energies were then fit parabolically to obtain the QCISD(T)/6-31G** equilibrium geometry $r_o=1.533$ Å, $R_p^o=0.511$ Å, $\phi_o'=110.976°$, and $D_e=96.26$ kcal/mol. This calculated geometry is in good agreement with the experimental neopentane geometry of $r_o=1.537$ Å, $\phi_o'=112°$, and is, thus, assumed to be an accurate description of the equilibrium geometry for the CH_3-^{t}Bu model. From $R_p^o=0.511$ Å, $\phi_{\rm eq}$ for Eq. (12) is found to be 109.336°, which reflects the near tetrahedral character of C_s, and $R_{\rm eq}$ for Eq. (12) is found to be 1.543 Å. The geometry about C_s is not perfectly tetrahedral because the H atoms attached to the C_1, C_2, and C_3 atoms are fixed in an eclipsed geometry [see Fig. 1(c)]. Values of $\phi_\infty=104.644°$ and $R_\infty=1.505$ Å are taken from the previous *ab initio* calculations for H$\cdot$ + ^{t}Bu.[22]

Besides giving an accurate CH_3-^{t}Bu geometry, the QCISD(T) calculations also give a good estimate of the CH_3-^{t}Bu bond energy. From the most recent experimental data,[72] the classical C-C bond dissociation energy D_e for neopentane is calculated to be 93.0 kcal/mol,[72–74] only 3 kcal/mol lower than the QCISD(T)/6-31G** bond energy for the CH_3-^{t}Bu model. Because the geometry of ^{t}Bu is constrained, D_e for CH_3-^{t}Bu will be larger than that for neopentane. This increase in D_e has been calculated as 0.9 kcal/mol,[50] and D_e for Eq. (10) was set to 93.9 kcal/mol.

B. Bending force constants

To complete the derivation of the potential energy function for reaction (9), f_ϕ^o, $f_{\phi'}^o$, and $f_{\theta'}^o$ force constants are needed for the CH_3-^{t}Bu equilibrium geometry [see Fig. 1(c)]. The f_θ force constant is a true constant, not attenuated, and is set to the diamond bulk C-C-C force constant of 0.868 mdyn Å/rad^2.[22,25]

1. ϕ bending force constant

The equilibrium C_m—C_s-C bending force constant f_ϕ^o was determined by the same procedure as described in Sec. III for deriving $f_\phi(r)$. The CH_3 geometry and ϕ' were held fixed, and the C_m—C_s-C angles bent by varying one of them by 5°. The energy was then calculated for this geometry at the QCISD(T)/6-31G** level of theory. The increase in the energy from the equilibrium geometry is due to ϕ bending motion and was fit to Eq. (24), with $f_\phi(r)$ and $\phi_o(r)$ replaced by f_ϕ^o and $\phi_{\rm eq}$, to give $f_\phi^o=1.15$ mdyn Å/rad^2. Reoptimizing the CH_3 geometry and ϕ' angles, after bending the ϕ angles, had an insignificant effect on the calculated energy and f_ϕ^o.

This fitted f_ϕ^o lies between 0.72 mdyn Å/rad^2 for H-C_s-C bending on a hydrogen-atom-terminated perfect diamond {111} surface,[22] and 1.26 mdyn Å/rad^2 for C-C—C bending in benzene.[68] Moreover, this fitted f_ϕ^o is in near exact agreement with 1.084 mdyn Å/rad^2 derived for a paraffin force field,[75] which included neopentane in the fit. Discrepancy with the MM3 (Ref. 54) value of 0.67 mdyn Å/rad^2 may lie in the fact that cycloalkanes, polycyclic structures, and unsaturated species were included in the fit, whereas the paraffin force field was fit to 270 fundamental experimental frequencies of saturated linear and branched hydrocarbons with an average error of 0.25%.

2. ϕ' bending force constant

The H-C_m—C_s $f_{\phi'}^o$ bending force constant was determined in a manner similar to that described above for f_ϕ^o. The ϕ angles were set to $\phi_{\rm eq}$, the CH_3 geometry held fixed, and the ϕ' angles displaced by varying one of them by 5°. The increase in energy with this ϕ' bending was calculated at the QCISD(T)/6-31G** level of theory and fit to an expression like Eq. (24). The fitted $f_{\phi'}^o$ of 0.59 mdyn Å/rad^2 agrees with the MM3 (Ref. 54) and paraffin force field[75] H-C-C force constants of 0.59 and 0.65 mdyn Å/rad^2, respectively.

3. θ' bending force constants

The H-C_m-H bending force constant $f_{\theta'}^o$ was calculated by displacing one of the H atoms, while holding the ϕ' angles and C-H bond lengths fixed, so that two of the θ' angles are changed by ~5°. The increase in energy was calculated at the QCISD(T)/6-31G** level and fit to the expression like Eq. (24). The resulting $f_{\theta'}=0.644$ mdyn Å/rad^2 is in good agreement with the MM3 (Ref. 54) and paraffin force field[75] H-C-H force constants of 0.55 and 0.543 mdyn Å/rad^2.

V. GENERAL ANALYTIC POTENTIAL FUNCTION FOR METHYL ADDITION TO DIAMOND SURFACES

A general analytic potential-energy function for $\cdot CH_3$ association with carbon-atom radical sites can be written as given in Eq. (5). $V_{\rm lattice}$ is a valence force field potential that has been fit to the diamond phonon spectrum, and $V_{\rm nonbonded}$ is described below. $V_{\rm CH_3,site}$ [see Fig. 1(c)] is written as the following function of the C_m—C_s separation r; i.e.,

$$V_{\rm CH_3,site}=V_{\rm radial}(r)+V_\phi(r)+V_{\phi'}(r)+V_\theta(r)+V_\gamma(r)+V_\chi(r)+V_R(r)+V_{\rm CH_3}(r), \quad (26)$$

where

$$V_{CH_3}(r) = V_{\theta'}(r) + V_{\Delta}(r) + V_{CH}. \quad (27)$$

The functional form and parameters for the terms in Eqs. (26) and (27) were given above in Secs. II and IV, and are summarized here.

The radial potential, $V_{radial}(r)$, is given by Eq. (10) with $D_e = 93.9$ kcal/mol, $r_o = 1.533$ Å, and β the quartic polynomial in Eq. (11). The angular potentials $V_{\phi}(r)$, $V_{\phi'}(r)$, $V_{\theta}(r)$, $V_{\gamma}(r)$, and $V_{\chi}(r)$ for the site are written as

$$V_X(r) = \frac{f_X(r)}{2} \sum_{i=1}^{3} [X_i - X_o(r)], \quad (28)$$

where $f_X(r)$ and $X_o(r)$ are the force constant and equilibrium geometry attenuated as a function of r. The ϕ and ϕ' angles are attenuated by Eq. (12), with the asymptotic limiting values $\phi_{\infty} = 104.644°$, $\phi_{eq} = 109.336°$, $\phi'_{\infty} = 90.000°$, and $\phi'_{eq} = 110.976°$. The $S_{\Delta\phi}$ and $S_{\Delta\phi'}$ switching functions are given by Eqs. (19) and (21), respectively. The attenuation of $f_{\phi'}(r)$ is given by Eq. (25) with $f^o_{\phi'} = 0.59$ mdyn Å/rad^2. Two different models are used for the $f_{\phi}(r)$ attenuation. For one, the attenuation is assumed to be the same as for $f_{\phi'}(r)$. For the other, the effect of the constrained ^{t}Bu geometry is considered, and the parameters in Eq. (25) are set to $a_1 = 0.390\,620\,534\,28$, $b_1 = 4.528\,131\,028\,3$ Å^{-2}, and $b_2 = 0.262\,492\,796\,38$ Å^{-5}. For the carbon-radical site on a diamond surface, the θ, γ, and χ are C-C-C angles, whose equilibrium values are related to $\phi_o(r)$ according to Eqs. (13)–(15). The f_{θ}, f_{γ}, and f_{χ} force constants are not attenuated, and are assigned the diamond C-C-C bending force constant of 0.868 mdyn Å/rad^2.[22,25] The C_s-C_1, -C_2, and -C_3 stretching potentials at the site are expressed by

$$V_R(r) = D_R \sum_{i=1}^{3} \{1 - \exp(-\beta_R[R_i - R_o(r)])\}^2, \quad (29)$$

with $D_R = 79.46$ kcal/mol and $\beta_R = 1.858$ Å^{-1}.[22]

The methyl potential, Eq. (27), consists of H-C-H θ' bending terms, the out-of-plane bend Δ term, and C-H stretching terms. The θ' potential is given by Eq. (28), with $\theta'_o(r)$ attenuated by Eq. (12) with $\theta'_{\infty} = 120.0°$, and $\theta'_{eq} = 107.925°$. The $S_{\Delta\theta'}$ switching function is given by Eq. (23). The asymptotic values for the $f_{\theta'}$ force constant are $f^o_{\theta'} = 0.644$ mdyn Å/rad^2 and $f^{\infty}_{\theta'} = 0.440$ mdyn Å/rad^2. The latter is the H-C-H bending force constant for the methyl radical. Parameters for $V_{\Delta}(r)$, the methyl out-of-plane bending potential, as well as the definition of Δ, are described in Ref. 44:

$$V_{\Delta}(r) = f_{\Delta}(r) \sum_{i=1}^{3} \Delta_i^2. \quad (30)$$

The asymptotic values for f_{Δ} are 0.0436 mdyn Å/rad^2 with CH_3 at infinite separation, and 0 with CH_3 attached to the surface. The attenuation of $f_{\theta'}(r)$ and $f_{\Delta}(r)$ between their asymptotic limits, was assumed to vary with $\Delta r = r - r_o$ in the same way as for $H + CH_3$ association.[44] V_{CH} is represented by the Morse function

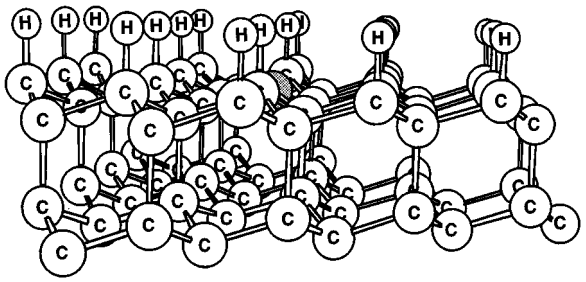

FIG. 6. The (12+10)-ring model used to represent the diamond {111} terrace site. The radical site is represented as a shaded atom.

$$V_{CH} = D_e^{CH}\{1 - \exp(-\beta_e^{CH}[R^{CH} - R_o^{CH}])\}^2, \quad (31)$$

with $R_o^{CH} = 1.1$ Å, $\beta_e^{CH} = 1.879$ Å^{-1}, and $D_e^{CH} = 110.6$ kcal/mol taken from Ref. 44.

$V_{nonbonded}$ in Eq. (5) describes the nonbonded interactions between the methyl radical atoms and the hydrogen atoms terminating the diamond surface and the carbon atoms in the top layer of the surface (i.e., the surface carbon atoms). The nonbonded C—C and H—C potentials are represented by the EXP-6 function of Williams and Starr,[76]

$$V = \frac{A}{r^6} + B \exp(-Cr) \quad (32)$$

with $A_{C—C} = -576.96$ Å^{-6}, $B_{C—C} = 877\,74.86$ kcal/mol, and $C_{C—C} = 3.60$ Å^{-1}, and $A_{H—C} = -136.9503$ Å^{-6}, $B_{H—C} = 15651.29$ kcal/mol, and $C_{H—C} = 3.67$ Å^{-1}. The H—H nonbonded potential is identical to that of Eqs. (5)–(8) in Ref. 22.

The above analytic potential, identified as MAPS/MeDIAM, was used to determine the optimized geometry and adsorption energy for $\cdot CH_3$ associating with a diamond {111} surface that has a carbon-atom radical site $\cdot C_s$. The (12+10)-ring model, shown in Fig. 6, was used to represent $\cdot C_s$ and the diamond lattice. Tests showed that the optimized geometry and adsorption energy are converged with this size model and do not change if larger models are used. The C_m-C_s bond length r for the optimized geometry is 1.571 Å and the H-C_m-C_s ϕ' angle is 112.848°. The classical adsorption energy is 77.0 kcal/mol. It is 16.9 kcal/mol smaller than D_e of 93.9 kcal/mol for $V_{CH_3,site}$ because of repulsions between H and C atoms of the CH_3 moiety and H and C atoms on the diamond surface.

The above results can be compared with those determined from electronic structure theory calculations for $\cdot CH_3$ adsorption with a radical site on the diamond {111} surface. The value calculated for the classical adsorption energy ranges from 62 to 104 kcal/mol. The atom-superposition and electron delocalization molecular-orbital method[77] gave a value of 71 kcal/mol. Two different local-density-approximation (LDA) calculations gave 99.2 (Ref. 78) and 103.8 kcal/mol.[51] A Möller-Plesset second-order perturbation theory (MP2)/6-31G**/6-31G calculation[49] gave values of 99.9 and 82.5 kcal/mol, without and with corrections for

basis-set superposition effects (BSSE's). A value of 61.8 kcal/mol was obtained from a density-functional theory (DFT) calculation.[79] The adsorption energy from the MP2 calculation with corrections for BSSE is in best agreement with the value of 77.0 kcal/mol calculated here. A difference of 10 kcal/mol between the adsorption energy of a methyl group on $\cdot^t$Bu and that of a methyl radical on the {111} surface was determined from HF/3-21G/STO-3G calculations,[49] which is somewhat smaller than the 16.9 kcal/mol found here.

The C_m-C_s bond length r is found to be 1.545, 1.563, and 1.74 Å from LDA,[51] MP2,[49] and DFT (Ref. 79) calculations, respectively, in comparison with the analytic potential value of 1.571 Å. The optimized ϕ' value from the MP2 calculation is 112.8°, while that determined from the analytic potential is 112.848°.

VI. KINETICS OF METHYL ADDITION TO A DIAMOND {111} TERRACE

The analytic potential-energy function derived here, MPAS/MeDIAM, may be used in classical trajectory and variational translational-state theory calculations of rate constants for methyl radical association with carbon-atom radical sites on diamond surfaces. Below, this potential is used to calculate the rate constant for $\cdot CH_3$ association with the diamond{111} surface. In future work,[80] the potential will be used to compare methyl association rate constants for different diamond radical sites.

A. Theoretical method and rate constant

Variational translation-state theory (VTST) has proven useful for calculating rate constants for radical-radical recombination reactions.[22,39,81] Because these processes are barrierless, a variational method is used to determine the TS structure. In canonical VTST (CVTST), the system's free energy is computed along the reaction path. To find the reaction path on an analytic potential energy function for a barrierless association reaction like CH_3+diamond {111}, the reaction path trajectory in mass-weighted Cartesian coordinates[41–43] is initialized with a large separation between the reactants with the remaining coordinates optimized. If the initial separation is sufficiently large, the resulting reaction path is independent of the starting separation.[82,83] The TS is then located at the free-energy maximum, which minimizes the rate constant.[39,84,85] In CVTST calculations based on the reaction path Hamiltonian,[41–43] normal-mode vibrational frequencies are calculated along the reaction path, and statistical thermodynamics is used to determine the free energy maximum.[39]

The CVTST calculations reported here for CH_3+diamond {111} association use the reaction path Hamiltonian and were performed with the MAPS/MeDIAM analytic potential added to VENUS96.[86] The CVTST rate constant is given by

$$k_{\mathrm{CVTST}}=\frac{k_B T}{h}\frac{Q^{\ddagger}}{Q_s Q_{\mathrm{Me}}}\exp(-E_o^{\ddagger}/k_B T), \tag{33}$$

where $Q^{\ddagger}$, Q_s, and Q_{Me} are the partition functions for the TS, surface, and methyl radical, respectively. $E_o^{\ddagger}$ is the potential-energy difference between the TS and reactants. All vibrational modes are treated as separable harmonic oscillators in the calculations, except the low-frequency CH_3 internal rotation at the TS and other points along the reaction path. Its partition function was calculated using the hindered internal rotor model described by Truhlar,[87] with an internal rotation symmetry number of 3. Because of the low frequency for the TS CH_3 internal rotation, it is near the free rotor limit. External rotational degrees of freedom do not contribute to $Q^{\ddagger}$ and Q_s. In previous work, the CVTST calculational approach used here has given accurate rate constants for H+CH_3 and H+diamond {111} association as compared to classical trajectory calculations.[22,40]

CVTST rate constants for CH_3+diamond {111} were computed between 300 and 2000 K, a temperature range representative of the experiments.[20,21,88–90] The calculations were performed with the (12+10)-ring model in Fig. 6 for the carbon-atom radical site and the diamond lattice. Two models were used for $S_\phi(r)$, given by Eq. (25), which is the switching function for the attenuation of the C_m—C_s-C $f_\phi(r)$ force constant. For one model the parameters for $S_\phi(r)$ are the same as those for $S_{\phi'}(r)$, the switching function for the H-C_m—C_s bending force constant. For the second, the parameters are adjusted (see Sec. III D) to take into account the effect of CH_3 associating with a surface radical site, whose motion is somewhat constrained by the rigid structure of the diamond lattice. Plots of these two models for $S_\phi(r)$ are shown in Fig. 5.

The calculated rate constants and some properties of the variational transition states are listed in Table II. The rate constant is seen to decrease by approximately a factor of 17 as the temperature is increased. There is an 11% difference between the rate constants calculated for the two $S_\phi(r)$ models. As has been found for the other associations,[22,40,82,91] the transition state tightens, i.e., $r^{\ddagger}$ decreases, as the temperature is increased. During the association of a methyl radical with a diamond surface, five vibrational modes called transitional modes[92] are created [see Fig. 1(c) for reference]. They are two C-C-C ϕ-type bending motions of the methyl radical, two H-C-C ϕ'-type rocking motions of the methyl radical, and a methyl radical torsion. In addition, the frequency for the CH_3 umbrella motion, which becomes a H-C-H deformation when CH_3 has associated, increases significantly. For CH_3 association with a symmetric site on the diamond {111} surface, both the ϕ and ϕ'-type motions are doubly degenerate. The frequencies for the transitional modes and the CH_3 umbrella mode at the variational transition states are listed in Table II.

B. Discussion

There have been no experimental measurements of the rate constant for $\cdot CH_3$ association with the diamond {111} surface or any diamond surface site. Thus direct comparison with experimental kinetic data is not possible. Moreover, experimental gas-phase rate constants involving methyl radical association are very scarce. Hwang, Wagner, and Wolff[93] report a temperature-dependent methyl radical recombination rate constant of $1.15\times10^{15}/T^{0.6}$ cm^3 mol^{-1} s^{-1} between 1200 and 1600 K, which equals 1.6×10^{13} cm^3 mol^{-1} s^{-1} at 1200 K. Zaslonko and Smirnov[94] found the expression $2.50\times10^{14}/T^{0.38}$ cm^3 mol^{-1} s^{-1} for temperatures in the range of

TABLE II. CVTST rate constants and transition-state proprties for CH_3+diamond {111} association.

	Model 1 (unconstrained)[a]					Model 2 (constrained)[b]				
T (K)	$r^{\ddagger c}$	$\nu^{\ddagger d}$	$E_o^{\ddagger e}$	$\Delta G^{\ddagger f}$	k_{CVTST}[g]	$r^{\ddagger}$	$\nu^{\ddagger}$	$E_o^{\ddagger}$	$\Delta G^{\ddagger}$	k_{CVTST}
300	3.34	39, 60(2) 206(2), 511	−4.1	3.93	0.89	3.34	39, 60(2) 206(2), 511	−4.1	3.93	0.88
1000	3.03	54, 101(2) 318(2), 710	−7.1	20.1	0.083	3.02	55, 106(2) 323(2), 714	−7.3	20.3	20.3
1500	2.91	62, 121(2) 371(2), 778	−9.2	32.3	0.063	2.91	63, 123(2) 373(2), 781	−9.3	32.6	0.057
2000	2.83	68, 141(2) 411(2), 830	−11.2	44.5	0.057	2.82	69, 147(2) 413(2), 835	−11.3	45.0	0.051

[a]Results obtained with Eq. (25) and the ϕ attenuation identical to that for association of two ethane molecules (see text).
[B]Results obtained with Eq. (25) and the previous ϕ attenuation scaled to model the geometry constraint (see text).
[c]C_m—C_s bond length at the transition state in Å.
[d]Torsion, C_m—C_s-C bend (2), H-C_m—C_s bend (2), and C_mH_3 umbrella transitional modes in cm^{-1}. Degeneracies are indicated in parentheses.
[e]Difference in classical potential energy between the transition state and reactants in kcal/mol.
[f]Free energy of activation in kcal/mol. Standard state is 1 mol/liter. The external symmetry number ratio between the reactants and transition state is 6, and is included in $\Delta G^{\ddagger}$.
[g]CVTST rate constant in units of 10^{10} L mol^{-1} s^{-1}.

300–1750 K, which gives 1.7×10^{13} cm^3 mol^{-1} s^{-1} at 1200 K. The temperature-dependent gas-phase rate constant for recombination of tertiary butyl radicals is reported[95] as $3.13\times10^{16}/T^{1.73}$ cm^3 mol^{-1} s^{-1} for temperatures of 300–1000 K, which gives a 1000-K rate constant of 0.02×10^{13} cm^3 mol^{-1} s^{-1}. It is interesting to note that both the CH_3 and ^{t}Bu recombination rate constants decrease with temperature as does the one calculated here for CH_3+diamond {111} association.

If chemical similarity is assumed, the rate constant for $\cdot CH_3$ and $\cdot{}^t$Bu [as well as $\cdot CH_3$+diamond {111}] recombination is expected to lie between those for methyl and tertiary butyl radical self-association. The values calculated here for the $\cdot CH_3$+diamond {111} association rate constants (Table II) are consistent with this statement. In a kinetic study of diamond growth, Goodwin[96] used a rate constant of 0.33×10^{13} cm^3 mol^{-1} s^{-1} for methyl recombination with diamond surface radical sites at 1200 K. This value is based on a molecular-dynamics simulation of H-atom collisions with the diamond {111} surface, using the Brenner potential,[97] and the Harris[98] mechanism for diamond growth. A recent study[57] showed limitations of the Brenner potential in modeling diamond growth, since the TS for bond breaking and/or bond forming occurs at longer ranges than the potential cutoff used by Brenner. For methyl radical association with the diamond {111} surface, Frenklach used for all surface sites a rate constant of 1.0×10^{13} cm^3 mol^{-1} s^{-1},[99] a value typical for barrierless gas-phase recombinations.[100] This rate constant is appreciably larger than that calculated here for $\cdot CH_3$+diamond {111} association.

The free energies of activation $\Delta G^{\ddagger}$ for H· and $\cdot CH_3$ association with the diamond {111} surface are nearly linear with temperature (see Fig. 7). This effect has been studied previously and an analytic function for $\Delta G^{\ddagger}(T)$ has been derived for gas-surface reactions.[101]

VII. CONCLUSIONS

In this work, transferable potential-energy surface properties for alkyl radical associations, experimental data, and high-level *ab initio* calculations are used to develop an analytic potential energy function for $\cdot CH_3$ association with carbon-atom radical sites on diamond surfaces. Future improvements of the potential will include refining the attenuation of bending forces as $\cdot CH_3$ associates. However, the current form of the potential is sufficiently accurate to give

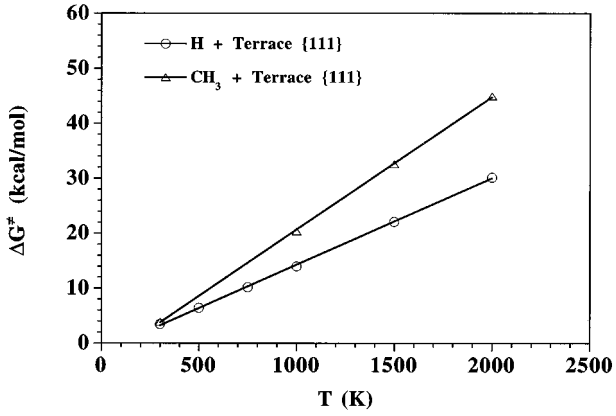

FIG. 7. Plots of $\Delta G^{\ddagger}$ vs temperature for association of hydrogen and methyl radicals to a diamond {111} terrace radical site. The $\Delta G^{\ddagger}$ values for methyl associaiton are for the unconstrained model (see Table II).

meaningful rate constants for $\cdot CH_3$ association with different diamond surfaces radical sites. This is significant since rate constants for $\cdot CH_3$ association with radical sites on diamond surfaces are needed in mechanisms for diamond film growth by chemical vapor deposition. These rate constants have not been determined experimentally and are expected to be particularly difficult to measure. Thus theoretical and/or computational studies are particularly important for determining CH_3+diamond association rate constants, as well as other rate constants involving diamond surfaces.

The potential developed here is used in a CVTST calculation, based on the reaction path Hamiltonian, to determine the $\cdot CH_3$+diamond {111} rate constant. At 1500 K, the calculated rate constant is approximately 0.06×10^{10} L mol^{-1} s^{-1}. In future work, the potential will be used in both CVTST and trajectory calculations of CH_3 association with C-atom radical sites on the {111}, {110}, and {100} diamond surfaces and at defect sites (e.g., steps, kinks, islands, and protrusions) on these surfaces.[102]

ACKNOWLEDGMENTS

This research was supported by the National Science Foundation. The MAPS/MeDIAM analytic potential developed here was added to the general computer program VENUS96. This modified version of VENUS96 is available through the Physics Auxiliary Publication Service.

[1] J. C. Angus, H. A. Will, and W. J. Stanko, J. Appl. Phys. **39**, 2915 (1968).
[2] B. V. Derjaguin and D. V. Fedoseev, Sci. Am. **233** N5, 102 (1975).
[3] S. Matsumoto, Y. Sato, M. Kamo, and N. Setaka, Jpn. J. Appl. Phys. **21**, L183 (1982).
[4] S. Matsumoto, Y. Sato, M. Tsutsumi, and N. Setaka, J. Mater. Sci. **17**, 3106 (1982).
[5] R. C. DeVries, Annu. Rev. Mater. Sci. **17**, 161 (1987).
[6] J. C. Angus and C. C. Hayman, Science **241**, 913 (1988).
[7] K. E. Spear, J. Am. Ceram. Soc. **72**, 171 (1989).
[8] W. A. Yarbrough and R. Messier, Science **247**, 688 (1990).
[9] F. J. Celii and J. E. Butler, Annu. Rev. Phys. Chem. **42**, 643 (1991).
[10] B. V. Derjaguin and D. V. Fedoseev, Russ. Chem. Rev. **39**, 783 (1970).
[11] D. V. Fedoseev, V. P. Varnin, and B. V. Derjaguin, Russ. Chem. Rev. **53**, 435 (1984).
[12] B. V. Spitsyn, L. L. Bouilov, and B. V. Derjaguin, J. Cryst. Growth **52**, 219 (1981).
[13] M. Frenklach, in *Diamond on Diamond-like Films and Coatings*, Vol. 266 of *NATO Advanced Study Institute Series B: Physics*, edited by R. E. Clausing, L. L. Horton, J. C. Angus, and P. Koidl (Plenum, New York, 1991), pp. 499–524.
[14] S. J. Harris, Appl. Phys. Lett. **56**, 2298 (1990).
[15] M. Frenklach, in *Proceedings of the 2nd International Symposium on Diamond Materials*, edited by A. J. Purdes, J. C. Angus, R. F. Davis, B. M. Meyerson, K. E. Spear, and M. Yoder (The Electrochemical Society, Pennington, NJ, 1991), pp. 142–153.
[16] J. E. Butler and R. L. Woodin, Philos. Trans. R. Soc. London Ser. A **342**, 209 (1993).
[17] M. Frenklach, S. Skokov, and B. Weiner, Nature (London) **372**, 534 (1994).
[18] W. R. L. Lambrecht, C. H. Lee, B. Segall, J. C. Angus, Z. Li, and M. Sunkara, Nature (London) **364**, 607 (1993).
[19] B. J. Garrison, E. J. Dawnkaski, D. Srivastava, and D. W. Brenner, Science **255**, 835 (1992).
[20] L. N. Drasnoperov, I. J. Kalinovski, H.-N. Chu, and D. Gutman, J. Phys. Chem. **97**, 11 787 (1993).
[21] B. D. Thoms, J. N. Russell, Jr., P. E. Pehrsson, and J. E. Butler, J. Chem. Phys. **100**, 8425 (1994).
[22] P. de Sainte Claire, P. Barbarat, and W. L. Hase, J. Chem. Phys. **101**, 2476 (1994).
[23] K. Song, P. de Sainte Claire, W. L. Hase, and K. C. Hass, Phys. Rev. B **52**, 2949 (1995).
[24] M. D. Perry and L. M. Raff, J. Phys. Chem. **98**, 4375 (1994); M. D. Perry and L. M. Rafff, *ibid.* **98**, 8128 (1994).
[25] M. Frenklach, J. Chem. Phys. **97**, 5794 (1992).
[26] M. Frenklach, in *Synthetic Diamond: Emerging CVD Science and Technology*, edited by K. E. Spear and J. P. Dismukes (The Electrochemical Society, Pennington, NJ, 1994); Chap. 8, p. 267.
[27] M. Frenklach and K. E. Spear, J. Mater. Res. **3**, 133 (1988).
[28] M. Frenklach, J. Appl. Phys. **65**, 5142 (1989).
[29] D. N. Belton and S. J. Harris, J. Chem. Phys. **96**, 2371 (1992).
[30] M. Frenklach and H. Wang, Phys. Rev. B **43**, 1520 (1991).
[31] M. Tsuda, M. Nakajima, and S. Oikawa, J. Am. Chem. Soc. **108**, 5780 (1986); Jpn. J. Appl. Phys. **26**, L527 (1987).
[32] D. Huang and M. Frenklach, J. Phys. Chem. **96**, 1868 (1992).
[33] D. Huang and M. Frenklach, J. Phys. Chem. **95**, 3692 (1991).
[34] W. L. Hase, D. G. Buckowski, and K. N. Swamy, J. Phys. Chem. **87**, 2754 (1983).
[35] K. C. Hass, M. A. Tamor, T. R. Anthony, and W. F. Banholzer, Phys. Rev. B **45**, 7171 (1992).
[36] M. J. Frisch, G. W. Trucks, H. B. Schlegel, P. M. W. Gill, B. G. Johnson, M. A. Robb, J. R. Cheeseman, T. Keith, G. A. Petersson, J. A. Montgomery, K. Raghavachari, M. A. Al-Laham, V. G. Zakrzewski, J. V. Ortiz, J. B. Foresman, J. Cioslowski, B. B. Stefanov, A. Nanayakkara, M. Challacombe, C. Y. Peng, P. Y. Ayala, W. Chen, M. W. Wong, J. L. Andres, E. S. Replogle, R. Gomperts, R. L. Martin, D. J. Fox, J. S. Binkley, D. J. Defrees, J. Baker, J. P. Stewart, M. Head-Gordon, C. Gonzalez, and J. A. Pople, GAUSSIAN 94, Revision C.3 (Gaussian, Inc., Pittsburgh, PA, 1995).
[37] J. A. Pople, M. Head-Gordon, and K. Raghavachari, J. Chem. Phys. **87**, 5968 (1987).
[38] R. G. Gilbert and S. C. Smith, *Theory of Unimolecular and Recombination Reactions* (Blackwell Scientific, Oxford, 1990).
[39] W. L. Hase and D. M. Wardlaw, in *Advances in Gas-Phase Photochemistry and Kinetics, Bimolecular Collisions*, edited by M. N. R. Ashfold and J. E. Baggott (Burlington, London, 1989), p. 171.
[40] X. Hu and W. L. Hase, J. Chem. Phys. **95**, 8073 (1991).
[41] W. H. Miller, N. C. Handy, and J. E. Adams, J. Chem. Phys. **72**, 99 (1980).
[42] S. Kato and K. Morokuma, J. Chem. Phys. **73**, 3900 (1980).

[43] A. D. Isaacson and D. G. Truhlar, J. Chem. Phys. **76**, 1380 (1982).
[44] R. J. Duchovic, W. L. Hase, and H. B. Schlegel, J. Phys. Chem. **88**, 1339 (1984).
[45] D. M. Hirst, Chem. Phys. Lett. **122**, 225 (1985).
[46] R. J. Wolf, D. S. Bhatia, and W. L. Hase, Chem. Phys. Lett. **132**, 493 (1986).
[47] S. H. Robertson, D. M. Wardlaw, and D. M. Hirst, J. Chem. Phys. **99**, 7748 (1993).
[48] M. W. Wong, A. Pross, and L. Radom, Isr. J. Chem. **33**, 415 (1993).
[49] K. Larsson, S. Lunell, and J.-O. Carlsson, Phys. Rev. B **48**, 2666 (1993).
[50] M. Page and D. W. Brenner, J. Am. Chem. Soc. **113**, 3270 (1991).
[51] M. R. Pederson, K. A. Jackson, and W. E. Pickett, Phys. Rev. B **44**, 3891 (1991).
[52] X. G. Zhao, C. S. Carmer, B. Wiener, and M. Frenklach, J. Phys. Chem. **97**, 1639 (1993).
[53] B. H. Besler, W. L. Hase, and K. C. Hass, J. Phys. Chem. **96**, 9369 (1992).
[54] N. L. Allinger, Y. H. Yuh, and J.-H. Lii, J. Am. Chem. Soc. **111**, 8551 (1989).
[55] J. Tersoff, Phys. Rev. Lett. **61**, 2879 (1988).
[56] D. W. Brenner, Phys. Rev. B **42**, 9458 (1990).
[57] P. de Sainte Claire, K. Song, W. L. Hase, and D. W. Brenner, J. Phys. Chem. **100**, 1761 (1996).
[58] Class-I force fields are represented by diagonal, quadratic terms, whereas class-II force fields, often derived from *ab initio* calculations, contain nondiagonal quadratic and higher-order anharmonic terms; M.-J. Hwang, T. P. Stockfisch, and A. T. Hagler, J. Am. Chem. Soc. **116**, 2515 (1994).
[59] S. J. Weiner, P. A. Kollman, D. T. Nguyen, and D. A. Case, J. Comput. Chem. **7**, 230 (1986).
[60] L. Nilsson and M. Karplus, J. Comput. Chem. **7**, 591 (1986).
[61] A. T. Hagler, P. S. Stern, S. Lifson, and S. Ariel, J. Am. Chem. Soc. **101**, 813 (1979).
[62] M. J. Hwang, T. P. Stockfisch, and A. T. Hagler, J. Am. Chem. Soc. **116**, 2515 (1994).
[63] J. R. Maple, M.-J. Hwang, T. P. Stockfisch, U. Dinur, M. Waldman, C. S. Ewig, and A. T. Hagler, J. Comput. Chem. **15**, 162 (1994).
[64] I. N. Levine, in *Quantum Chemistry*, 4th ed. (Prentice-Hall, Englewood Cliffs, NJ, 07632), Chap. 13.
[65] F. B. Brown and D. G. Truhlar, Chem. Phys. Lett. **113**, 441 (1985).
[66] M. Rittby and R. J. Bartlett, J. Phys. Chem. **92**, 3033 (1988); G. Scuseria, Chem. Phys. Lett. **176**, 27 (1991).
[67] P. C. Hariharan and J. A. Pople, Theor. Chim. Acta **28**, 213 (1973), and references cited therein. M. M. Francl, W. J. Peitro, W. J. Hehre, J. S. Binkley, M. S. Gordon, D. J. DeFrees, and J. A. Pople, J. Chem. Phys. **77**, 3654 (1982); M. J. Frisch, J. A. Pople, and J. S. Binkley, *ibid.* **80**, 3265 (1984), and references cited therein.
[68] P. J. Nagy and W. L. Hase, Chem. Phys. Lett. **54**, 73 (1978).
[69] H. B. Schlegel, J. Chem. Phys. **84**, 4530 (1986); P. J. Knowles and N. C. Handy, *ibid.* **88**, 6991 (1988).
[70] This switching function may also be represented by $1-\tanh[\alpha\Delta r(\Delta r-\beta)^6]$, where $\alpha=2.939\,465\,091\times10^{-8}$ Å^{-7} and $\beta=-16.573\,083\,505$ Å.
[71] L. S. Bartell and W. F. Bradford, J. Mol. Struct. **37**, 113 (1977).
[72] D_e for the C-C bond in neopentane was calculated from the experimental bond enthalpy at 298 K of 87.3 kcal/mol (Ref. 73) and a consistent set of fundamental frequencies proposed for $C(CH_3)_4$, $C(CH_3)_3$, and CH_3 (Ref. 74). The bond enthalpy at 0 K is calculated to be 85.3 kcal/mol.
[73] *CRC Handbook of Chemistry and Physics*, 75th ed., edited by D. R. Lide (Chemical Rubber, Boca Raton, FL, 1993).
[74] I. G. Pitt, R. G. G. Gilbert, and K. R. Ryan, J. Phys. Chem. **99**, 239 (1995).
[75] J. H. Schachtschneider and R. G. Snyder, Spectrochim. Acta **19**, 117 (1963).
[76] D. E. Williams and T. L. Starr, J. Comput. Chem. **1**, 173 (1977).
[77] S. P. Mehandru and A. B. Andersson, J. Mater. Res. **5**, 2286 (1990).
[78] J. W. Mintmire, in *Proceedings of the 2nd International Conference on the New Diamond Science and Technology*, edited by R. Messier and J. Glass, MRS Symposia Proceedings No. 162 (Materials Research Society, Pittsburgh, 1991).
[79] D. R. Alfonso, S. H. Yang, and D. A. Drabold, Phys. Rev. B **50**, 15 369 (1994).
[80] P. de Sainte Claire and W. L. Hase (unpublished).
[81] W. L. Hase, S. L. Mondro, R. J. Duchovic, and D. M. Hirst, J. Am. Chem. Soc. **109**, 2916 (1987).
[82] S. N. Rai and D. G. Truhlar, J. Chem. Phys. **79**, 6046 (1983).
[83] W. L. Hase and R. J. Duchovic, J. Chem. Phys. **83**, 3448 (1985).
[84] D. G. Truhlar and B. C. Garrett, Acc. Chem. Res. **13**, 440 (1980).
[85] D. G. Truhlar, W. L. Hase, and J. T. Hynes, J. Phys. Chem. **87**, 2644 (1983).
[86] W. L. Hase, R. J. Duchovic, X. Hu, A. Komornicki, K. F. Lim, D.-H. Lu, G. H. Peslherbe, K. N. Swamy, S. R. Vande Linde, A. J. C. Varandas, H. Wang, and R. J. Wolf, Quantum Chem. Program Exchange **16**, 671 (1996). VENUS96 is an enhanced version of MERCURY [W. L. Hase, *ibid.* **3**, 453 (1983)].
[87] D. G. Truhlar, J. Comput. Chem. **12**, 266 (1991).
[88] S. J. Harris and D. G. Goodwin, J. Phys. Chem. **97**, 23 (1993).
[89] W. L. Hsu, Appl. Phys. Lett. **59**, 1427 (1991).
[90] W. L. Hsu, J. Appl. Phys. **72**, 3102 (1992).
[91] W. L. Hase, J. Chem. Phys. **64**, 2442 (1976).
[92] Y. N. Lin and B. S. Rabinovitch, J. Phys. Chem. **74**, 3151 (1970).
[93] S. M. Hwang, H. Gg. Wanger, and Th. Wolff, in *23rd International Symposium on Combustion* (Combustion Institute, Pittsburgh, 1990), Vol. 94.
[94] I. S. Zaslonko and V. N. Smirnov, Kinet. Katal **20**, 575 (1979).
[95] D. L. Baulch, C. J. Cobos, R. A. Cox, P. Frank, G. Hayman, Th. Just, J. A. Kerr, T. Murrells, M. J. Pilling, J. Troe, R. W. Walker, and J. Warnatz, J. Phys. Chem. Ref. Data **23**, 1026 (1994); N. L. Arthur, J. Chem. Soc. Faraday Trans. **82**, 1057 (1986).
[96] D. G. Goodwin, J. Appl. Phys. **74**, 6888 (1993).
[97] D. W. Brenner, D. H. Robertson, R. J. Carty, D. Srivastava, and B. J. Garrison, in *Computational Methods in Materials Science*, edited by J. E. Mark, M. E. Glicksman, and S. P. Marsh, MRS Symposia Proceedings No. 278 (Materials Research Society, Pittsburgh, 1992), p. 255.
[98] S. J. Harris and D. G. Goodwin, J. Phys. Chem. **97**, 23 (1993); S. J. Harris, Appl. Phys. Lett. **56**, 2298 (1990).
[99] S. Skokov, B. Weiner, and M. Frenklach, J. Phys. Chem. **98**, 7073 (1994).
[100] W. G. Mallard, F. Westley, J. T. Herron, R. F. Hampson, and D. H. Frizzell, *NIST Chemical Kinetics Database 5.0* (National In-

stitute of Standards and Technology, Gaithersburg, MD, 1993).
[101] P. de Sainte Claire, W. L. Hase, G. H. Peslherbe, and H. Wang, J. Am. Chem. Soc. **119**, 5007 (1997).
[102] See AIP Document No. E-PAPS: E-PRBMDO-56-13 543-MB for a brief description of material or figures. E-PAPS document files may be retrieved free of charge from our FTP server (http://www.aip.org.lepaps/epaps.html). For further information, e-mail: paps@aip.org; or fax: 516-576-2223.